Impact of building density on natural ventilation potential and cooling energy saving across Chinese climate zones

Article

Accepted Version

Xie, X. ORCID: https://orcid.org/0000-0003-2280-1768, Luo, Z. ORCID: https://orcid.org/0000-0002-2082-3958, Grimmond, S. ORCID: https://orcid.org/0000-0002-3166-9415 and Sun, T. ORCID: https://orcid.org/0000-0002-2486-6146 (2023) Impact of building density on natural ventilation potential and cooling energy saving across Chinese climate zones. Building and Environment, 244. 110621. ISSN 0360-1323 doi: 10.1016/j.buildenv.2023.110621 Available at https://centaur.reading.ac.uk/113596/

To link to this article DOI: http://dx.doi.org/10.1016/j.buildenv.2023.110621

Publisher: Elsevier

https://doi.org/10.1016/j.buildenv.2023.110621

Impact of building density on natural ventilation potential and cooling energy saving across Chinese climate zones

Xiaoxiong Xie [a], Zhiwen Luo [b] *, Sue Grimmond [c], Ting Sun [d]

[a] School of the Built Environment, University of Reading, UK [b] Welsh School of Architecture, Cardiff University, UK
[c] Department of Meteorology, University of Reading, UK [d] Institute for Risk and Disaster Reduction, Univ. College London, UK

*Corresponding author: Prof Zhiwen Luo; Email: LuoZ18@Cardiff.ac.uk

Abstract

Natural ventilation is an energy-efficient approach to reduce the need for mechanical ventilation and air conditioning in buildings. However, traditionally weather data for building energy simulation are obtained from rural areas, which do not reflect the urban micrometeorological conditions. This study combines the Surface Urban Energy and Water Balance Scheme (SUEWS) and EnergyPlus to predict natural ventilation potential (NVP) and cooling energy saving in three idealised urban neighbourhoods with different urban densities in five Chinese cities of different climate zones. SUEWS downscales the meteorological inputs required by EnergyPlus, including air temperature, relative humidity, and wind speed profiles. The findings indicate that NVP and cooling energy saving differences between urban and rural areas are climate- and season-dependent. During summer, the urban-rural differences in natural ventilation hours are -43% to 10% (cf. rural) across all climates, while in spring/autumn, they range from -7% to 36%. The study also suggests that single-sided ventilation can be as effective as cross ventilation for buildings in dense urban areas. Our findings highlight the importance of considering local or neighbourhood-scale climate when evaluating NVP. We demonstrate a method to enhance NVP prediction accuracy in urban regions using EnergyPlus, which can contribute to achieving low-carbon building design.

Keywords: Natural ventilation, urban climate, land surface model, EnergyPlus, climate zone

Nomenclature

A	Effective opening area (m^2)
C_d	Discharge coefficient of opening
C_p	Wind pressure coefficient
g	Gravitational acceleration ($m\ s^{-2}$)
$h_{opening}$	Height of opening (m)
P_w	Wind pressure (Pa)
Q_{saving}	Cooling energy saving (J)
T	Air temperature (°C)
U	Wind speed ($m\ s^{-1}$)
V	Ventilation rate ($m^3\ s^{-1}$)
α	Wind profile exponent
δ	Height where a constant mean gradient wind speed is assumed to occur (m)
λ_P	Plan area fraction
ρ_0	Outdoor air density ($kg\ m^{-3}$)

subscripts

b	Buoyancy-driven
w	Wind-driven
ref	Reference condition at the meteorological station

1. Introduction

The Paris Agreement calls on countries to cut carbon emissions to meet the target of limiting global warming to preferably 1.5 °C compared to pre-industrial levels (UN, 2015). In 2019, carbon emissions from the operation of buildings accounted for 28% of total global energy-related carbon emissions (UNEP, 2020). Although in China building operation contributes to 21.6 % of national carbon emissions (CABEE, 2021), China's building energy consumption is expected to continue to rise with urbanisation and climate change. Thus, it is important but challenging to improve energy efficiency.

Natural ventilation is a key passive cooling strategy used to achieve low-carbon building design. It reduces energy consumption, and improves occupants' health, comfort, and productivity (Emmerich et al., 2001). As the effectiveness of natural ventilation depends on the outdoor weather conditions, these impacts need to be assessed.

Natural ventilation potential (NVP) is defined as the possibility (or probability) of achieving acceptable indoor thermal comfort and air quality through natural ventilation alone (Luo et al., 2007). Although studied worldwide using different methods and metrics (Table 1), assessing NVP can be difficult due to its sensitivity to factors such as weather, climate, building design, and the surrounding environment (Yin et al., 2010). Current methods can be generally categorised into climate-based and building simulation approaches (Wang and Malkawi, 2019).

Climate-based approaches provide broad geographic NVP variations using outdoor air temperature and wind speed (Wang and Malkawi, 2019), for use in the early design stage when detailed building information is unavailable (outdoor data analysis, Table 1). For example, Chen et al.'s (2017) global analysis using typical meteorological year (TMY) data found temperate climates (e.g. subtropical highland, Mediterranean) tend to have larger NVP compared to more extreme climates (e.g. tropical, subarctic). Humidity has also been identified as being important when assessing NVP in hot-humid climates (Causone, 2016).

Using building energy simulation tools (e.g. EnergyPlus (U.S. Department of Energy, 2020a), TRNSYS (2009), DeST (Yan et al., 2008), IES-VE (Integrated Environmental Solutions, 2018)) NVP assessments can account for building design elements (building simulation, Table 1) including impacts such as the internal heat gain, building envelope, occupancy schedule and ventilation pattern. In comparison to climate-based approaches, building simulations can mitigate uncertainties arising from building location and design. Numerous studies (Anđelković et al., 2016; Fumo et al., 2010; Lam et al., 2014; Royapoor and Roskilly, 2015; Ryan and Sanquist, 2012) have demonstrated the capability of building energy simulation tools to accurately model indoor thermal environments (hourly biases < 10% for energy consumption and < 1.5 °C for indoor air temperature), given that detailed and precise input data are available. Therefore, it is crucial to use appropriate weather data inputs for building energy simulation purposes (Hensen, 1999).

Originally (and typically) building energy simulation tools treat buildings as being isolated, using weather data input acquired from meteorological stations located in open country. However, the climate in urban areas is known to differ from surrounding rural areas due to various aspects of the urban environment potentially affecting natural ventilation (Oke et al., 2017a), as shown in Fig. 1. Under wind-driven ventilation conditions the airflow pattern is influenced by surrounding buildings modifying the wind pressure on building facades (van Hooff and Blocken, 2010; Yang et al., 2008; Zhang et al., 2005). Whilst buoyancy-driven ventilation is affected by warmer outdoor air temperatures caused by the canopy layer urban heat island effect (WMO, 2023), which is a result of the building fabric affecting heat storage and waterproofing (Grimmond et al., 1986; Grimmond and Oke, 1999a), anthropogenic heat release from human activities (Allen et al., 2011; Sailor, 2011), trapped longwave radiation (Xie et al., 2022) and reduced wind speed (WMO, 2023).

Considering these impacts, employing a traditional approach that relies on rural weather data for building simulations in urban environments can introduce large biases in building energy performance, indoor thermal environment and natural ventilation rate. Previous studies explored these biases resulting from neglecting the impacts of urban factors. Neglecting increases in urban air temperature can cause biases of up to 11% in building energy consumption (Boccalatte et al., 2020; Kamal et al., 2021; Liu et al., 2017; Magli et al., 2015). For buildings situated in dense neighbourhoods (with a building plan area fraction (λ_P) of 0.6), neglecting the wind sheltering effect can overpredict the natural ventilation rate by as much as 19% (Xie et al., 2023), while overlooking the effect of inter-building longwave radiative exchange can underpredict the annual cooling energy by up to 17% (Xie et al., 2022). Such biases in natural ventilation rates and indoor thermal environments can influence the NVP assessment.

Some studies have accounted for urban climate when assessing NVP, with most using computational fluid dynamic (CFD) models (Table 1) to obtain air flow (Toparlar et al., 2017). However, CFD methods are dependent on the meteorological boundary conditions and the building morphology details, and their high computational costs make them unsuitable for long-term and large-scale simulations. Long-term modelling using EnergyPlus has accounted for urban climate, by modifying weather data using a simple urban heat island scenario that considers the air temperature only, so natural ventilation cooling energy savings can be simulated (Ramponi et al., 2014). However, their urban heat island (UHI) prediction only considers a fixed UHI magnitude, which does not account for neighbourhood density (or building plan area fraction), and thus may not fully represent the local climate. Tong et al. (2017) accounted for local atmospheric conditions on NVP for super high-rise buildings using Monin-Obukhov similarity theory (MOST) approach. However, MOST applies in the inertial sublayer (a layer that begins 2 to 5 times above the mean canopy height) if present but not in the roughness sublayer (Grimmond and Oke, 1999b; Theeuwes et al., 2019). Also, the analysis did not consider inter-buildings impacts such as radiation. In summary, the comprehensive consideration of all urban impacts shown in Fig. 1 when assessing NVP is currently limited in the existing literature.

To better account for urban impacts on NVP, in this study we propose a multi-scale modelling scheme by combining the urban land surface model Surface Urban Energy and Water Balance Scheme (SUEWS) (Järvi et al., 2011) and the building simulation tool EnergyPlus (U.S. Department of Energy, 2020a).

SUEWS uses commonly available surface characteristics and climate forcing data to simulate energy and water fluxes and derive local-scale environmental parameters (Järvi et al., 2011; Ward et al., 2016). It addresses the limitations of previous urban land surface models (Grimmond et al., 2011, 2010) by specifically addressing the better representation of latent heat flux and incorporating multiple sub-models to enhance accuracy (Järvi et al., 2011). The performance of SUEWS has been extensively evaluated in diverse global climates (see Table 3 of Lindberg et al. (2018); Table 1 of Sun and Grimmond (2019)), demonstrating its acceptable accuracy. Notably, Tang et al. (2021) evaluated SUEWS air temperature profile against observations at a central London site, considering two different heights above ground, and reported mean absolute errors (MAEs) of less than 1 °C. Furthermore, Theeuwes et al. (2019) compared the wind profile modelled with the modified MOST approach embedded in SUEWS with observations in Basel and Gothenburg, reporting MAEs ranging from 0.15 to 0.5 m s^{-1} at roof level. Applications of SUEWS in various urban environments worldwide have provided valuable insights. Researchers have used SUEWS to investigate the impacts of urbanisation on local climate (e.g. Fernández et al., 2021; Lindberg et al., 2020; Rafael et al., 2020) and building energy performance (Tang et al., 2021), assess the performance of green infrastructure (e.g. Havu et al., 2022; Wiegels et al., 2021), and analyse the effectiveness of different heat mitigation strategies (e.g. Augusto et al., 2020; Ward and Grimmond, 2017).

The open-source U.S. Department of Energy (2020a) EnergyPlus building energy simulation tool is one of the most widely used, and can be used for assessing natural ventilation potential (Table 1). Following extensive evaluation, EnergyPlus has been shown to accurately model the indoor thermal environment and natural ventilation given accurate and detailed input information. For example, Royapoor and Roskilly (2015) report a calibrated EnergyPlus model can predict annual hourly indoor air temperatures with an accuracy of ±1 °C for 93.2% of the time. Whilst, from comparing EnergyPlus Airflow Network (AFN) model results to experimental data Johnson et al. (2012) conclude the model errors are generally below 30%, which is deemed acceptable for analytical natural ventilation models (Zhai et al., 2016). Notably, for buoyancy-driven cross ventilation, the error falls below 10%. Although these errors are higher than for CFD modelling (less than 10% in neutral condition, i.e. no temperature variability, van Hooff et al., 2017), the advantages of AFN lie in having a better balance between accuracy and computational cost.

The SUEWS-EnergyPlus multiscale modelling scheme brings several advantages compared to previous studies. First, both models have undergone rigorous evaluations, ensuring their reliability and accuracy. Second, SUEWS has a modified MOST model (Harman and Finnigan, 2007; Tang et al., 2021; Theeuwes et al., 2019) providing vertical profiles within the roughness sublayer (RSL) of temperature, wind, and relative humidity for where the buildings are located. Third, the scheme takes into account the impact of wind sheltering effects by incorporating local wind profiles and correspondingly modified wind pressure coefficient data (Xie et al., 2023). Fourth, the scheme considers the influence of inter-building longwave radiative exchanges (Xie et al., 2022). With all combined (also shown in Fig. 1), they create an effective, comprehensive multiscale modelling approach.

The objectives of this study are to: (1) improve EnergyPlus's ability to predict NVP in the urban environment, (2) analyse impacts of urban climate on the NVP, and (3) investigate how NVP changes with neighbourhood plan area fraction of buildings and climate.

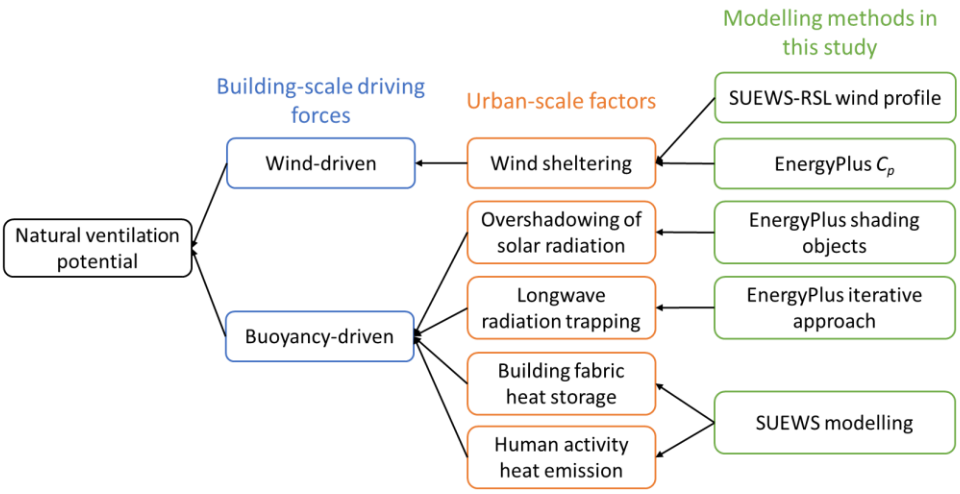

Fig. 1. Factors influencing natural ventilation potential in urban areas and the modelling methods used in this study. C_p: wind pressure coefficient.

Table 1: Summary of studies on natural ventilation potential (NVP) by date. Weather data source: open - standard rural meteorological station; urban - on-site observation or CFD modelling. NVP Metric: NV-hours - natural ventilation hours; PDPH - pressure difference Pascal hours; NVCE – natural ventilation cooling effectiveness (Yoon et al., 2020), ratio of actual ventilation heat loss rate to required ventilation heat loss rate. NV criteria: T - air temperature, U -wind; RH - relative humidity. Method of NVP calculation: OutMet – outdoor meteorological data, BS - Building simulation, OuInMet - Outdoor/indoor data analysis.

City Location	NVP Method	Effective NV criteria				BS tool	Weather data	NVP Metric	Urban Met	Reference
		T	*U*	*RH*	Others					
Townsville, Australia	OutMet	√	√	√		-	Open	Number of occasions		(Aynsley, 1999)
Multiple China	BS	√	√			Own model	Open	PDPH		(Yang et al., 2005)
Athens, Greece	OutMet	√	√		Noise, pollution	-	Urban	No metrics - Method development	*T, U*	(Ghiaus et al., 2006)
Multiple China	BS	√	√			Own model	Open	NV-hours, PDPH		(Luo et al., 2007)
Basel, Switzerland	OuInMet	√	√		Noise, pollution	-	Urban	NV-hours	*T, U*	(Germano, 2007)
Multiple China	BS	√				Own model	Open	NV-hours		(Yao et al., 2009)
Multiple China	BS	√	√	√		Own model	Open	NV-hours		(Yin et al., 2010)
Vejle, Denmark	BS	√				EnergyPlus	Open	NV-hours		(Oropeza-Perez and Østergaard, 2013)
Multiple Europe	OuInMet	√	√			-	Open	NV-hours		(Faggianelli et al., 2014)
Multiple China	BS	√		√		DeST and CFD	Urban	Mean ventilation rate	*T, RH*	(Li and Li, 2015)
Multiple India	BS	√	√			TRNSYS	Open	PDPH		(Patil and Kaushik, 2015)
Multiple US	BS	√				EnergyPlus	Open	Target air change rate		(Hiyama and Glicksman, 2015)
State College, US	BS	√	√			IES-VE	Open	NV-hours		(Cheng et al., 2016)
Multiple Global	OutMet	√		√		-	Open	NV-hours		(Causone, 2016)
Multiple China	BS	√		√	Pollution	EnergyPlus	Open	NV-hours		(Tong et al., 2016)
Multiple US	OutMet	√	√	√		-	Urban	NV-hours	*T, U, RH*	(Tong et al., 2017)
Multiple Europe	BS	√			Pollution	EnergyPlus	Open	NV-hours		(Martins and Carrilho Da Graça, 2017)
Multiple Global	OutMet	√	√			-	Open	NV-hours		(Chen et al., 2017)
Multiple Australia	BS	√				TRNSYS	Open	NV-hours		(Tan and Deng, 2017)
Multiple Spain	BS	√		√		DesignBuilder	Open	NV-hours		(Pesic et al., 2018)
Multiple North America	BS	√				Own model + CFD	Open	NV-hours		(Cheng et al., 2018)

Boston, US	BS	√	√			Own model + CFD	Urban	NV-hours	*T*, *U*	(Wang and Malkawi, 2019)
Multiple China	BS	√				EnergyPlus	Open	NV-hours		(Chen et al., 2019)
Chongqing, China	BS	√			Pollution	EnergyPlus + CFD	Urban	NV-hours	*T*	(Costanzo et al., 2019)
Multiple US	BS	√	√			EnergyPlus	Open	NVE		(Yoon et al., 2020)
Chambéry, France	BS	√	√			EnergyPlus	Open	NV-hours		(Sakiyama et al., 2021)

2. Methods

To study the impact of urban climate on building natural ventilation potential (NVP), we couple the local-scale land surface model Surface Urban Energy and Water Balance Scheme (SUEWS) v2021a (SuPy v2021.11.20) (Järvi et al., 2011; Sun et al., 2020; Sun and Grimmond, 2019; Tang et al., 2021; Ward et al., 2016) and the building energy simulation tool EnergyPlus v9.4 (U.S. Department of Energy, 2020a). Representative cities from five different climate zones in China are selected to consider the climate variations.

2.1. Urban neighbourhood scale climate modelling

The urban surroundings could affect the natural ventilation of a building of interest (Fig. 2) in multiple ways (Fig. 1) by directly impacting the driving potential of NV (buoyancy force and wind-driven force). Specifically, the street geometry in a neighbourhood can result in a decrease in wind speed, leading to a reduction in wind-driven natural ventilation rate. The canopy layer urban heat island (UHI) can lead to smaller temperature differences between indoor and outdoor air, which can reduce the buoyancy-driven natural ventilation rate. Here we use an urban neighbourhood wind profile, which requires the use of modified wind pressure coefficients based on differences between free-stream and urban neighbourhood wind profiles in EnergyPlus (Xie et al., 2023).

SUEWS is used to model three idealised neighbourhoods (Fig. 2) that have different building plan area densities but the same initial climate forcing data. The simulated energy and water balance fluxes are used to diagnose local-scale meteorological variables for the three neighbourhoods which are provided to EnergyPlus as the weather data for the building energy simulations. SUEWS performance has been extensively evaluated and applied in different climates globally (e.g. Table 3 of Lindberg et al. (2018); Table 1 of Sun and Grimmond (2019)).

SUEWS allow each neighbourhood to have varying amounts of seven land cover types: paved, buildings, deciduous trees/shrubs, evergreen trees/shrubs, grass, bare soil and water. This allows realistic intra-city land cover variations, between different cities. For simplicity, here we assume neighbourhoods consist of buildings and grass (i.e., two typical but contrasting surface types), so vegetation's influence (e.g., evapotranspiration) is considered but more complicated impacts, such as trees/shrubs influence on wind (Kent et al., 2018) and radiation (Morrison et al., 2018) are not included. Our three neighbourhoods are:
(a) *rural* (Fig. 2a): is a large area covered with 100% grass, hence the isolated building area is negligible
(b) *medium density* (Fig. 2b): has buildings covering 30% of the area (plan are fraction λ_P = 0.3) and grass covering 70%
(c) *high density* (Fig. 2c): has λ_P =0.6 and grass in the remaining 40% of the area

The SUEWS neighbourhood population density is consistent with the EnergyPlus building occupancy (Section 2.2).

The Design Standard for Energy Efficiency of Public Buildings (MoHURD, 2015) classifies China into five climate zones (Table 2) using typical average air temperatures in January and July as the primary indicators. This classification aims to provide guidance on the design of building envelope thermal characteristics for each specific climate zone and identifies the major cities in the zone. Here we use the ERA5 (ECMWF Reanalysis version 5) (Hersbach et al., 2020) meteorological data, which are available globally at a spatial resolution of 0.125° and a temporal resolution of a hour. As natural ventilation cooling for buildings is particularly important during hot periods, we select 2018, the year with the warmest Northeast Asia summer (JJA) mean near-surface air temperature between 1979 and 2018 (K. Xu et al., 2019) for simulation. The three neighbourhoods are simulated in one city for each of the five climates (Table 2), assuming human activities do not vary between the regions. One ERA5 grid located in centre of the city is used. Note the ERA5 data do not account for urban land cover in the reanalysis but do assimilate meteorological data with cities (Tang et al., 2021). The vegetation cover assigned to the grid is representative of local conditions (Hersbach et al., 2020).

To drive SUEWS the meteorological data in the inertial sub layer or constant flux layer are needed. This layer is located above the roughness sub layer (RSL). Within the RSL individual roughness element influences the air flow, while above that the flow becomes blended and provides a neighbourhood or local scale response. The RSL extends from ground to a depth of approximate 2 to 5 times of mean roughness element height (i.e. buildings and trees) (Oke et al., 2017b), where the building are located and most human activities occur. Thus, SUEWS forcing height depends on both the building height (i.e. height above ground level) and the city altitude (height above sea level, see Fig. 1 in Tang et al. 2020). With a mean building height is 6.4 m (Fig. 2) the forcing height above ground level (agl) needs to be at least 12.8 to 32 m agl. For example, central Kunming is located at an altitude of 1892 m above sea level (asl) (Liu et al., 2022), whereas the larger ERA5 grid-cell over central Kunming has an altitude of 2000 m asl (or 108 m agl). Therefore for Kunming a forcing height of 108 m agl is used. For climates with ERA5 height less than 32 m agl, The ERA5 data are adjusted to the appropriate height using the environmental lapse rate following Tang et al.'s (2021) Appendix B.

Building energy simulation of natural ventilation potential, requires wind speed *U*, air temperature *T* and relative humidity *RH* in the RSL. Here we use the SUEWS-RSL module to obtain the environmental variables. SUEWS-RSL calculates vertical profiles of these variables with a RSL corrected MOST (Monin-Obukhov Similarity Theory) approach (Harman and Finnigan, 2008, 2007; Theeuwes et al., 2019), while accounting for varying atmospheric stability, roughness characteristics and turbulent heat fluxes

(Tang et al., 2021; Theeuwes et al., 2019). Evaluation of the SUEWS-RSL *U* and *T* profiles against observations in three global cities, suggest an acceptable accuracy (Tang et al., 2021; Theeuwes et al., 2019).

The SUEWS-RSL generated local weather data, includes *T* and *RH* at 2 m above ground (T_2 and RH_2), *U* at 10 m (U_{10}), and vertical profiles of *T* and *U* within the RSL (Fig. 3). The supplied T_2, RH_2 and U_{10} as well as other climate data (e.g., incoming solar radiation from ERA5) are formatted as a EnergyPlus weather file (.epw). The SUEWS-RSL wind profile is passed to EnergyPlus via input files (.idf) by replacing the power law coefficients with values derived from the SUEWS-RSL data.

In EnergyPlus solar shading from adjacent buildings (purple, Fig. 2) are simulated as 'shading objects'. The longwave radiative exchanges between the reference building and adjacent buildings are calculated with an iterative approach (Xie et al., 2022). Impacts of other urban factors like the heat storage and the anthropogenic heat are simulated with SUEWS and accounted for in the outdoor air temperature (Fig. 1, Fig. 3).

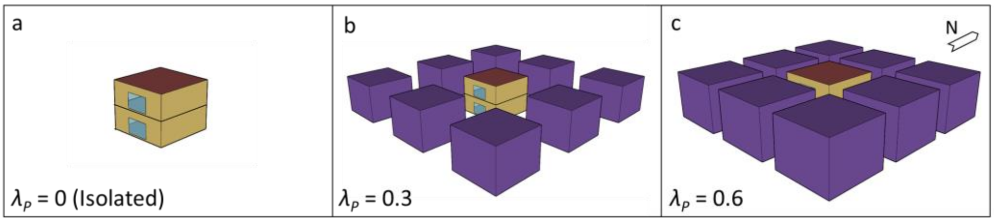

Fig. 2. Reference building (8 m × 8 m × 6.4 m) is simulated (EnergyPlus) after the weather data is simulated (SUEWS) for three neighbourhoods: (a) a rural (isolated), and two city neighbourhoods with building plan area fractions (λ_P) of (b) 0.3 and (c) 0.6.

Table 2. Building thermal characteristics and specific city simulated in each climate zones in China. SHGC: solar heat gain coefficient. Modified from Tong et al. (2016).

City	Climate zone	U-value (W m^{-2} K^{-1})				SHGC
		Roof	External wall	Ground floor	Window	Window
Harbin	Very cold	0.25	0.35	0.25	1.76	0.68
Beijing	Cold	0.39	0.46	0.46	1.77	0.37
Shanghai	Cold winter hot summer	0.39	0.54	0.46	2.3	0.32
Kunming	Temperate	0.44	0.72	1.32	2.4	0.2
Guangzhou	Warm winter hot summer	0.44	0.72	1.32	2.4	0.2

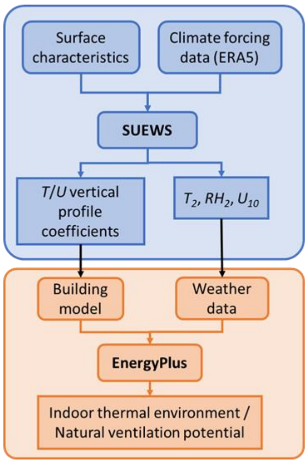

Fig. 3. Overview of the SUEWS-EnergyPlus workflow integration (Tang et al., 2021).

2.2. Building characteristics

To compare the NVP, a two-storey building model (Fig. 2a) based on ASHRAE Case 600 (ANSI/ASHRAE, 2011) is developed in EnergyPlus. The 8 m wide × 8 m long × 6.4 m tall, building has no interior partitions. There are two windows on each floor, one on the south-facing and one on the north facing-wall to provide natural ventilation. All four windows are 2 m × 3 m. A simplified residential occupancy (2 people on each floor, 125.6 W person^{-1}, occupied all-day) and internal heat gain (lighting: 6 W m^{-2}, equipment: 4.3 W m^{-2}) are assumed (Xiong et al., 2019). The simulated reference building is assigned the Design Standard for Energy Efficiency of Public Buildings (MoHURD, 2015) thermal characteristics appropriate for each climate zone (Table 2).

For the NVP analysis, we consider both cross and single-sided ventilation (only south-facing windows open). All windows are assumed to have 15% openable area and discharge coefficient (C_d) of 0.61. For the cooling energy savings calculation, an ideal load system is assumed with a heating setpoint of 18 °C and cooling setpoint of 26 °C based on the recommendation of the Code for Thermal Design of Civil Building (MoHURD, 2016).

2.3. Natural ventilation models

To simulate the cross ventilation the Airflow Network (AFN) model within EnergyPlus is used (U.S. Department of Energy, 2020b). The AFN has been evaluated and widely used for natural ventilation calculations (Johnson et al., 2012). The AFN airflow rate is calculated using the pressure difference across openings, with the standard orifice flow equation. The wind-driven ventilation rate V_w is (Awbi, 2003):

$$V_w = C_d A \sqrt{\frac{2\Delta P_w}{\rho_0}} \qquad (1)$$

where C_d is the discharge coefficient of opening, A is the effective opening area (m^2), ρ_0 is the outdoor air density (kg m^{-3}) and ΔP_w is the wind pressure difference across opening (Pa). The wind pressure at the opening height is (Awbi, 2003):

$$P_w = 0.5\rho_0 C_p U_{free}^2 \qquad (2)$$

where C_p is the surface-averaged wind pressure coefficient, and U_{free} is the upstream undisturbed flow at the opening height.

As C_p values are influenced by the building geometry, surrounding conditions and wind profile and direction (Grosso, 1992), it is important to use the appropriate C_p values as it impacts the accuracy of the building natural ventilation simulation in an urban environment. In this study, TPU *Aerodynamic Database of Non-isolated Low-Rise Buildings* (TPU, 2007) C_p data from wind-tunnel experiments for buildings with different geometries and surrounding conditions are used. As the TPU C_p database is for free-stream wind measured in wind tunnel experiments, we modified these using the SUEWS-RSL wind speeds and profile as shown in Xie et al. (2023).

Although it is widely accepted that cross ventilation usually achieves much larger ventilation rate, it is less practical than single-sided ventilation for urban buildings where isolated rooms are common (Zhong et al., 2022). The single-sided ventilation model, based on the mixing layer theory (Warren, 1977; Warren and Parkins, 1984), is used. This has been evaluated in wind-tunnel and full scale experiments (Gough et al., 2020; Yamanaka et al., 2006). The wind-driven ventilation rate (V_w, m^3 s^{-1}) is calculated with:

$$V_w = 0.1AU \qquad (3)$$

From Bernoulli principles, the buoyancy-driven ventilation rate (V_b) is calculated with:

$$V_b = \frac{C_d A}{3}\sqrt{g h_{opening}\frac{\Delta T}{T}} \qquad (4)$$

where g is the gravitational acceleration, $h_{opening}$ the height of the opening, ΔT air temperature difference across the opening. The total ventilation rate (V_t) is the quadrature sum of the wind and stack air flow components (U.S. Department of Energy, 2020c):

$$V_t = \sqrt{V_w^2 + V_b^2} \qquad (5)$$

2.4. Analysis metrics

In this study, the natural ventilation hours (NV-hour) and the cumulative air change rate (ACH-hour) are used to quantify the natural ventilation potential (NVP).

The NV-hour, the most common NVP metric (Table 1), is the number of hours per year when natural ventilation can fulfil both the air quality and thermal comfort requirements (Luo et al., 2007; Yin et al., 2010). ASHRAE Standard 62.1 (ANSI/ASHRAE, 2013) defines the required minimum outdoor airflow rate (V_R) for a residential space as a function of the number of people occupying (N_p) the floor area (A_f , units: m^2) as:

$$V_R = 0.0025N_p + 0.0003A_f \qquad (6)$$

In this study, as each floor has N_p = 2 and A_f = 64 m^2, V_R = 0.0242 m^3 s^{-1} (≈ 0.425 ACH).

For free-running building thermal comfort assessment, we use the Chinese adaptive thermal comfort models provided in the *Evaluation Standard for Indoor Thermal Environment in Civil Buildings* (MoHURD, 2012) for 75% satisfaction (or Category II). These specify an upper (T_{UL}) and lower indoor operative temperature limit (T_{LL}) by zone, with the northern (very cold, cold, Table 2):

$$\begin{cases} T_{UL,N} = 0.73T_{rm} + 15.28 & (18℃ \le T_{UL,N} \le 30℃) \\ T_{LL,N} = 0.91T_{rm} - 0.48 & (16℃ \le T_{LL,N} \le 28℃) \end{cases} \qquad (7)$$

and southern zones (cold winter hot summer, temperate, warm winter hot summer, Table 2):

$$\begin{cases} T_{UL,S} = 0.73T_{rm} + 12.72 & (18℃ \le T_{UL,S} \le 30℃) \\ T_{LL,S} = 0.91T_{rm} - 3.69 & (16℃ \le T_{LL,S} \le 28℃) \end{cases} \qquad (8)$$

This uses a seven day (n = 7) running mean of the outdoor air temperature (T_{rm}):

$$T_{rm} = (1-k)(T_{od-1} + \alpha T_{od-2} + \alpha^2 T_{od-3} \cdots + \alpha^6 T_{od-7}) \qquad (9)$$

where k is a constant between 0 and 1, with 0.8 as recommendation (Nicol and Humphreys, 2010), and T_{od-n} is the daily mean outdoor air temperature for n days ago (°C).

As higher ventilation rates may prevent sick building syndrome symptoms and reduce potential airborne infection risk (Sundell et al., 2011), we also determine the ACH-hour, or cumulative air change rate during the NV-hour period. This is similar to pressure difference Pascal hours (PDPH) (Yang et al., 2005). Although both aim to quantify availability of natural driving forces, ACH-hour is more directly linked to amount of ventilation.

Cooling energy saving (Q_{saving}) is also determined (Tong et al., 2016):

$$Q_{saving} = Q_{window\_closed} - Q_{window\_open} \qquad (10)$$

The is the difference in energy demand between a fully air-conditioned building (i.e. windows always closed, Q_{window_closed}) and a hybrid-controlled building with windows open (Q_{window_open}) when the indoor air temperature can vary between the heating and cooling set points (18 to 26 °C) while the air conditioning system is turned off. The air-conditioning system setting are given in section 2.1.

In summary (Fig. 4), three metrics are determined from analysis of simulations for five climates and for three neighbourhoods with different plan area fractions (λ_P) and two ventilation types. Thus, a total of (5 × 3 × 2 =) 30 cases are simulated.

We use mean the bias error (MBE) to assess the difference between SUEWS-RSL and modified EnergyPlus wind profiles (Eq. 12, Table 3 coefficients):

$$MBE = \frac{1}{N}\sum_{i=1}^{N}(y_i - x_i) \qquad (11)$$

where y_i and x_j are EnergyPlus and SUEWS-RSL wind speeds at each timestep, and N is the number of values analysed (i.e. a year with hourly timestep, N = 8760).

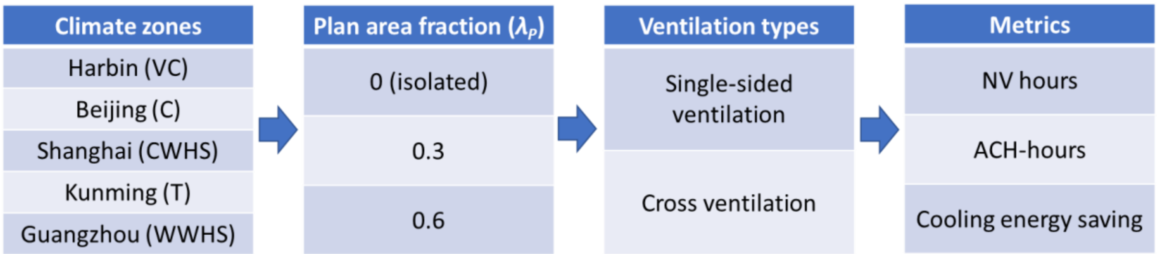

Fig. 4. Variables and metrics analysed in this study. See Fig. 2 and Table 2 for more details.

3. Results

3.1. Outdoor climate

First, we assess differences in modelled local environmental variables for the neighbourhoods with different building plan area fractions (λ_P) and in different climate zones (Fig. 4).

Modelled outdoor air temperature at 2 m (T_2) in denser neighbourhoods (larger λ_P, green Fig. 5) have warmer monthly values and greater variation than at the rural site in all five climates (blue, Fig. 5). Annual mean differences in T_2 between cases with λ_P of 0.6 and 0 vary between 0.8 ℃ in Guangzhou and 1.6 ℃ in Kunming. This difference is indicative of the canopy layer urban heat island effect.

Whereas the monthly variation of SUEWS-RWL modelled wind speed at 10 m (U_{10}) decrease as λ_P increases (Fig. 6). The annual mean differences ($\Delta\lambda_{P\ 0.6\rightarrow 0}$) are smallest in Beijing (0.6 m s^{-1}) to and larges in Harbin (1.1 m s^{-1}). These results are qualitatively similar to previous CFD studies considering outdoor velocity and λ_P (e.g. Mei et al. (2017)).

Vertical wind profiles (Fig. 7) derived SUEWS-RSL are used to calculate the EnergyPlus power-law parameters (δ, α, Table 3)(ASHRAE, 2005):

$$U_z = U_{10}\left(\frac{\delta_{ref}}{10}\right)^{\alpha_{ref}}\left(\frac{z}{\delta}\right)^{\alpha} \qquad (12)$$

where the meteorological station boundary layer depth (δ_{ref}) and exponent (α_{ref}) are obtained as the default settings in EnergyPlus for open terrain (U.S. Department of Energy, 2020d).

To assess the mean bias error (MBE) for the EnergyPlus wind profiles when using the Table 3 coefficients (hereafter EP-RSL profiles), we use the original SUEWS-RSL vertical wind profiles data which varying because of the different forcing heights; (5 to 8 vertical levels for λ_P = 0; 9 levels at λ_P = 0.3 and 0.6) as the baseline (Fig. 8). As the SUEWS-RSL wind profile does not assume a power law and varies with stability (Tang et al., 2021; Theeuwes et al., 2019), biases still exist in EP-RSL profiles. The biases are larger for climates with stronger wind speeds (e.g. Harbin). When λ_P = 0, the EP-RSL profiles underpredicts the median wind speeds by up to 0.35 m s^{-1}, especially around 2 m above ground level. For λ_P = 0.3 the EP-RSL MBE_{median} are smaller (≤ 0.2 m s^{-1}), as are λ_P = 0.6 cases. As the MBE_{median} become better (smaller) with height within the canopy layer (> 3.2 m), we focus analysis on the upper floor natural ventilation potential and energy saving. Future work could directly use the RSL wind profile within EnergyPlus after rewriting the appropriate code. This is beyond the scope of this study.

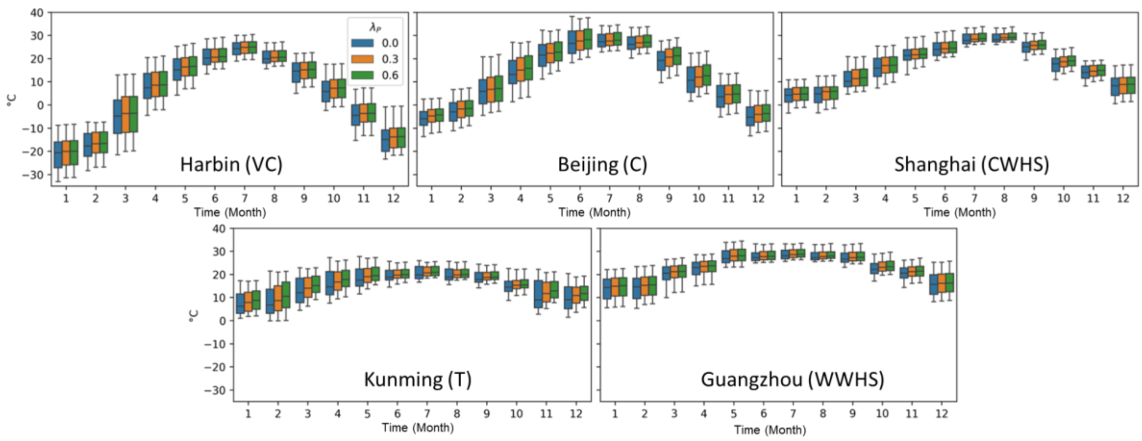

Fig. 5. Monthly distribution (hourly) of modelled outdoor air temperature at 2 m agl for three plan area fraction of buildings (λ_P, Fig. 2; colours)

and five climates (Table 2), with interquartile range (box), median (horizontal line) and 5th and 95th percentiles (whiskers).

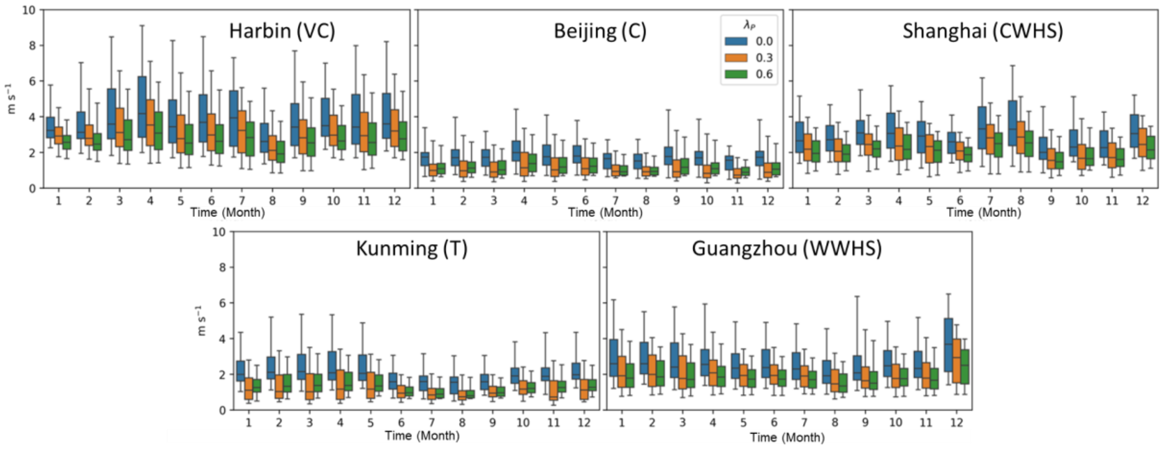

Fig. 6. As Fig. 5, but wind speed at 10 m agl.

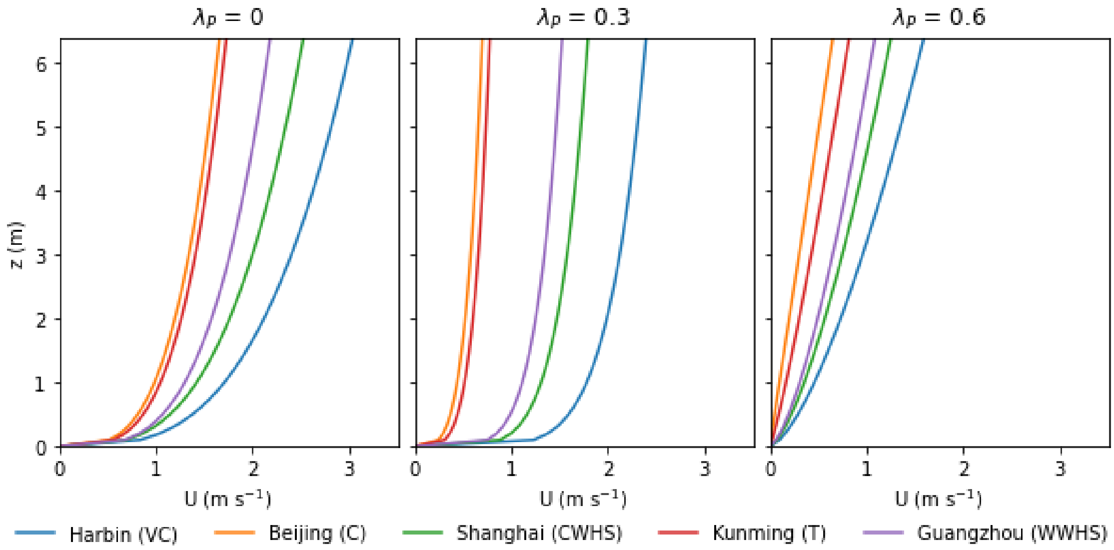

Fig. 7. Vertical wind profiles for three different λ_P and five climates (colour) calculated with annual median 10 m wind speeds and coefficients (Table 3) derived from the SUEWS-RSL results (EP_{RSL}) within the canopy layer (building height= 6.4 m).

Table 3: Wind power law (Eq. 12) coefficients derived from SUEWS-RSL model output for each climate and neighbourhood.

	Exponent α					Boundary layer depth δ (m)				
λ_P	Harbin (VC)	Beijing (C)	Shanghai (CWHS)	Kunming (T)	Guangzhou (WWHS)	Harbin (VC)	Beijing (C)	Shanghai (CWHS)	Kunming (T)	Guangzhou (WWHS)
0	0.31	0.28	0.31	0.27	0.28	40.41	37.88	37.34	46.62	46.93
0.3	0.16	0.25	0.17	0.22	0.17	380.44	125.28	322.01	149.76	320.19
0.6	0.67	1.02	0.68	0.86	0.68	25.96	16.16	25.11	16.65	24.87

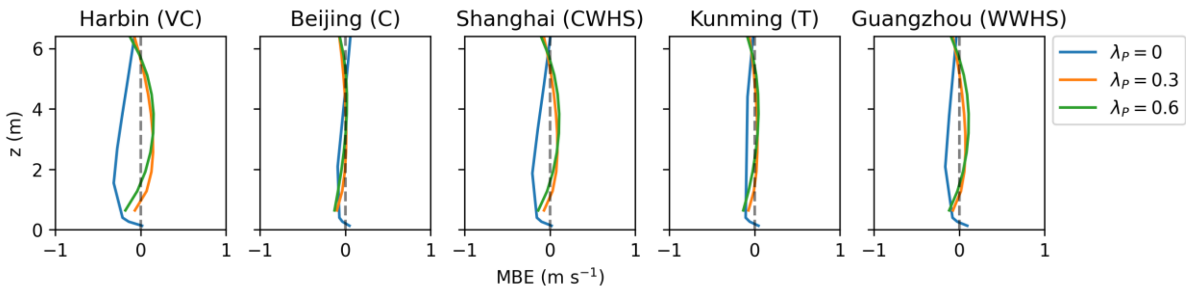

Fig. 8. Annual mean bias error (MBE) for wind speed calculated at hourly timestep but vertical resolution (Δz) that varies (from 0.13 m with varying Δz for $\lambda_P = 0$; from 0.64 m with Δz= 0.64 m for $\lambda_P = 0.3$ and 0.6) to 6 m above ground level; where SUEWS-RSL (*x*, Eq. 11) and EP-RSL wind profiles (*y*, Eq11; using Eq. 12, and Table 3 coefficients) for three λ_P (colour) and five climates.

3.2. Natural ventilation potential (NVP)

3.2.1. Natural ventilation hours (NV-hour) of cross ventilation

Cross ventilation monthly percentage of NV-hours across the five climates (Table 2) and three λ_P classes (Fig. 2) are generally larger for upper floor room (Fig. 9). With windows always opened, the minimum ventilation rate requirement of 0.425 air change per hour (ACH) (section 2.4) can be fulfilled during most of the year (Fig. 9). Although the Beijing neighbourhood with $\lambda_P = 0.6$

has the lowest wind speeds, there are only 23 hours within the year that do not meet the ventilation rate criteria. Thus, differences in NV-hours are mostly influenced by the thermal comfort criteria. As a result, warm climates (Guangzhou, Kunming, Shanghai) have more annual total NV-hours than cold climates (Harbin, Beijing), since there is very limited NV potential for cold climates in winter (Fig. 9).

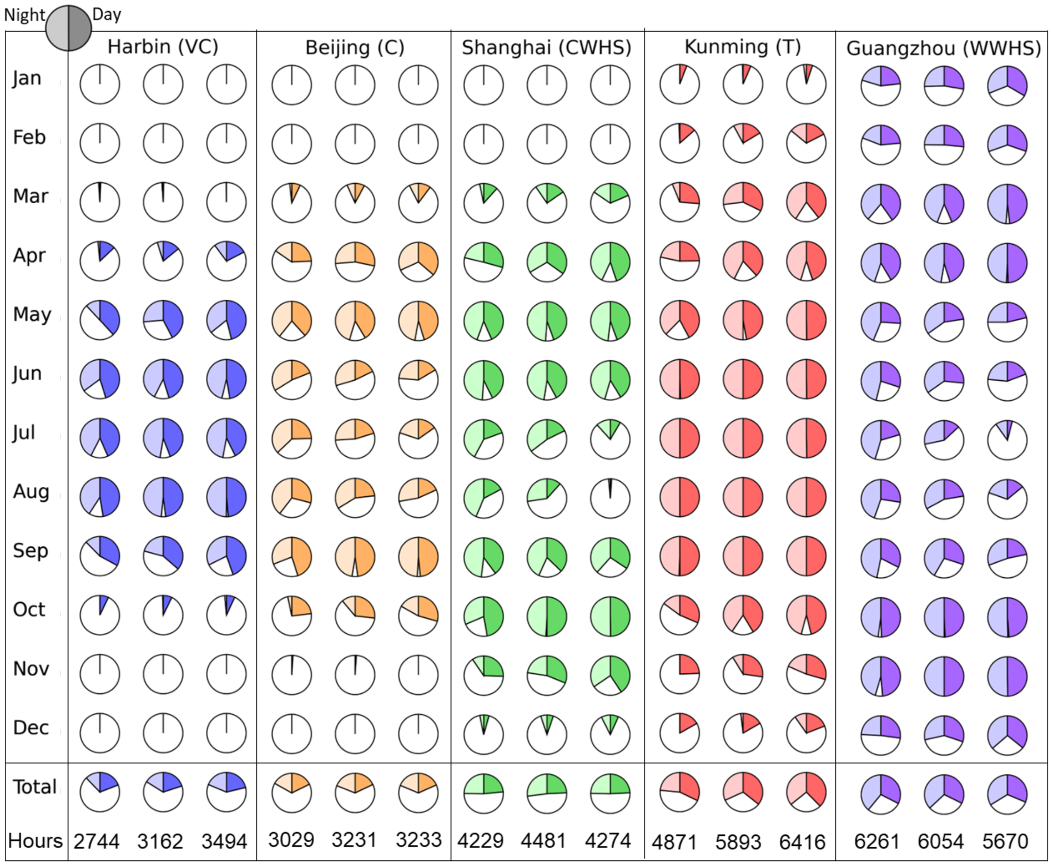

Fig. 9. Upper floor cross ventilation as percentages of NV-hours (relative to total hours in the period for five climates (columns), three neighbourhoods (λ_P colours, blue: 0; green: 0.3; red: 0.6) and different time intervals (rows: monthly and annual, time of day (pie chart half): right daytime (7:00 to 19:00), left night-time (19:00 to 7:00)).

Influences of λ_P on NV-hours vary across climates (Fig. 9). In terms of the annual total, the building in the $\lambda_P = 0$ rural neighbourhood has the most annual NV-hours in hot climates like Guangzhou. While for low-medium density $\lambda_P = 0.3$, warm winter hot summer climates like Shanghai have the most annual NV-hours. Dense urban neighbourhoods ($\lambda_P = 0.6$) have the most annual NV-hours in cold northern zones including Harbin and Beijing, and the mild climates like Kunming. This can be explained by the air temperature distribution (Fig. 6) as dense neighbourhoods ($\lambda_P = 0.6$) tend to have higher outdoor temperatures (in their regional climate), which is beneficial in cool climates for thermal comfort, and vice versa. The annual differences in NV-hours between $\lambda_P = 0$ and $\lambda_P = 0.6$ is largest in Kunming (1545) which is more than twice the difference to the next largest (Harbin, 753). The others are smaller again Guangzhou (587), Shanghai (254), and smallest in Beijing (201).

The λ_P has a greater impact on nocturnal NV-hours than daytime (Fig. 9), linked to the larger night-time temperature differences (Fig. 5). During cool months there are larger proportion of daytime NV-hours, but the nocturnal NV-hours increases with λ_P to a greater extent (e.g. nocturnal NV-hours increase by 33.9% while daytime increase by 13.2% from $\lambda_P = 0$ to 0.6 during March in Kunming). While in warm months, nocturnal NV-hours are reduced more with the increase of λ_P (e.g. nocturnal NV-hours decrease by 35.3% while daytime increase by 16.3% from $\lambda_P = 0$ to 0.6 during July in Guangzhou).

Generally, the dependence of NV-hours change with λ_P is highly related to climate and seasons (Fig. 10). In summer, very cold climates (e.g. Harbin) have an increase in NV-hours with λ_P (10% $\lambda_P = 0.6$ c.f. $\lambda_P = 0$), while the opposite occurs in hot summer climates regions (-43% $\lambda_P = 0.6$ c.f. $\lambda_P = 0$ in Guangzhou). Whereas in the temperate climate (e.g. Kunming) λ_P has negligible impact on NV-hours, as temperatures have both small variations and are usually pleasant for indoor thermal comfort (Fig. 9). In winter, NV-hours increase with λ_P in all regions due to cooler outdoor air temperatures, but the increase is small in regions with cold winter and little natural ventilation potential including Harbin, Beijing and Shanghai. During the spring/autumn transition seasons, the NV-hours tend to increase with λ_P in most climates associated with the relatively mild outdoor climate except Guangzhou, where the warm climate causes the indoor air temperature to exceed the upper limit of thermal comfort in late spring (May) and early autumn (September) (Fig. 9).

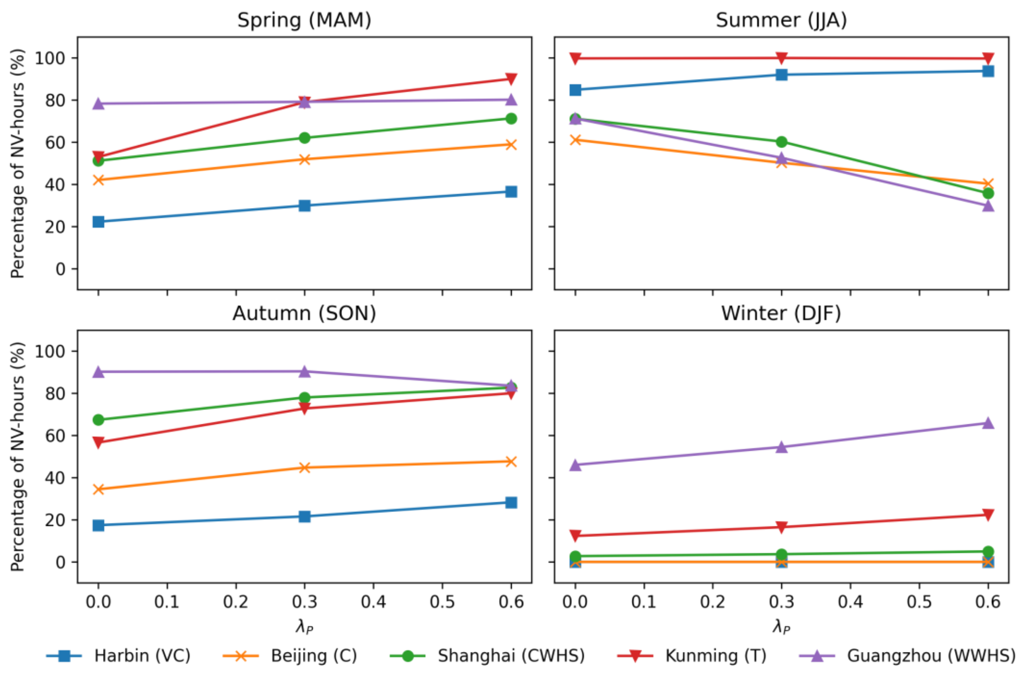

Fig. 10. Seasonal upper floor with cross ventilation (**percentage of NV hours**) in five climates (colour) for three λ_P (marker).

3.2.2. ACH-hours of cross ventilation

The air exchange rates can enhance the NV benefits for air quality purposes. The annual variability in ACH (hourly) during NV period (Fig. 11) is the largest when buildings are sited in open areas (λ_P = 0) because of the higher variability of wind speed (Fig. 6 and 8), with median ACH between 10.8 (Beijing) and 20 (Harbin). As λ_P increases the median ACHs become smaller (λ_P = 0.3: 4.9 (Beijing) and 10.1 (Harbin); λ_P = 0.6: 2.6 (Beijing) and 3.0 (Harbin)).

The annual cumulative ACH-hours differs from NV-hours with λ_P variations. As ACH-hours largely depend on wind speeds and ACH-hours decrease with λ_P in all climates (Fig. 12), the inter-climate variations are smaller (Fig. 12). Given the large number of annual NV-hours, buildings in areas with a λ_P of 0 and 0.3 in Guangzhou and λ_P = 0.6 in Kunming have the most ACH-hours (cf. to buildings in the same λ_P neighbourhoods but different climates). While Beijing has the least annual ACH-hours for all λ_P due to low both ventilation rate and NV-hours.

The seasonal variations in ACH-hours are also influenced by both NV-hours and ventilation rates (Fig. 13). In transition seasons (spring/autumn), Guangzhou's climate has the largest ventilation potential in both ACH-hours and NV-hours (Fig. 10) benefiting from appropriate air temperatures and wind speeds, while Kunming's ranking drops due to the low ventilation rates. In summer, high wind speeds and mild summer temperatures make Harbin the climate with the most ACH-hours. The ranking of ACH-hours in winter remains consistent with the NV-hours.

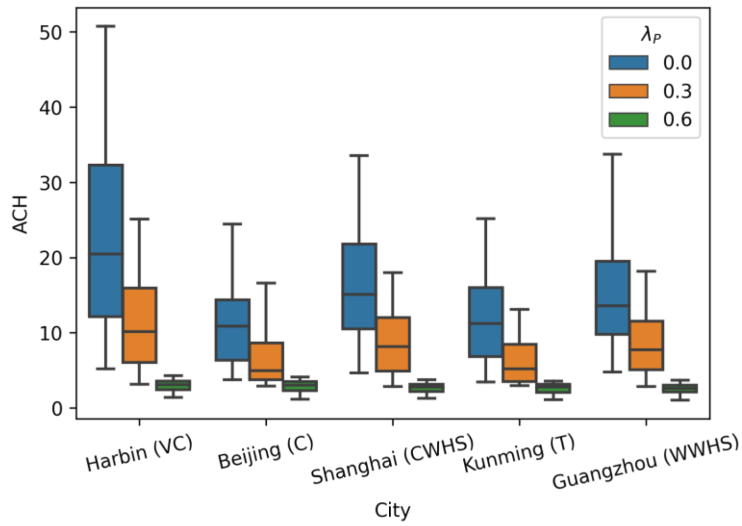

Fig. 11. Annual variability in air changes per hour (ACH) when the upper floor cross ventilation (NV-hour >0) through the year for five climates and three λ_P (colours) with interquartile range (box), median (horizontal line) and 5[th] and 95[th] percentiles (whiskers).

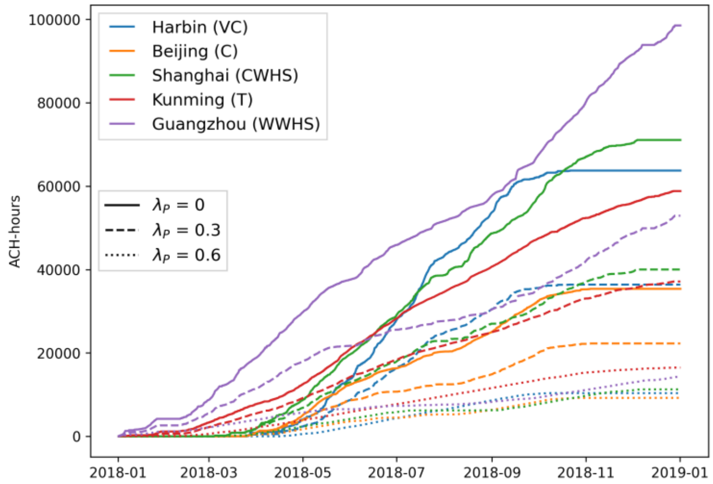

Fig. 12. Annual cumulative ACH-hours of the upper floor with cross ventilation across different climates (colour) and λ_P (line style).

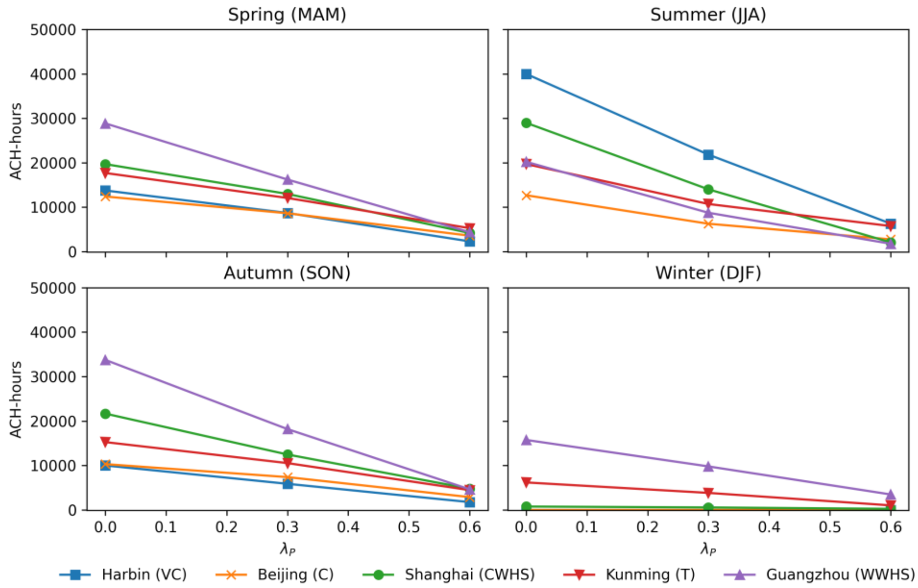

Fig. 13. Seasonal upper floor **ACH-hours** with cross ventilation in five climates (colour) for three λ_P (marker).

3.2.3. Single sided ventilation

To assess NVP differences between cross ventilation and single-sided ventilation we focus on Shanghai as similar conclusions are drawn for the other cities. Ventilation rates are largely less for single-sided ventilation (cf. cross ventilation) (Fig. 14) with annual median ACH reducing from 15.1/8.2/2.7 (cross ventilation) to 3.9/2.9/2.1 (single-sided ventilation) across the three plan area densities (λ_P = 0/0.3/0.6). This also implies that the single-sided ventilation is as effective as cross ventilation for buildings located in dense urban areas. Although the ventilation rates are reduced, the annual minimum ventilation rate for the single-sided ventilation building even for λ_P = 0.6 (0.59 ACH), still meets the requirement of indoor air quality. Therefore, in Shanghai the natural ventilation potential is mainly influenced by thermal comfort criteria only. However, we do not consider the impact of outdoor air pollution (i.e., assuming outdoor air is unpolluted).

The reduced ventilation cooling potential with single-sided ventilation causes median indoor air temperature to increase by 0.9/0.8/0.2 °C for λ_P = 0/0.3/0.6 (Fig. 14). The seasonal percentage of NV-hours with single-sided ventilation therefore increases by up to 10.6 % (λ_P = 0) during spring and autumn, but decreases by up to 14.7 % (λ_P = 0.3) in summer (cf. cross ventilation) (Fig. 15). The ACH-hours are higher with cross ventilation in all conditions due to the higher ventilation rate, and differences between ventilation modes decreases as λ_P increases (Fig. 16).

Generally, the single-sided ventilation leads to lower ventilation rates across λ_P, and reduce the natural ventilation potential in magnitude. The changing pattern of NVP with λ_P is similar to cross ventilation,

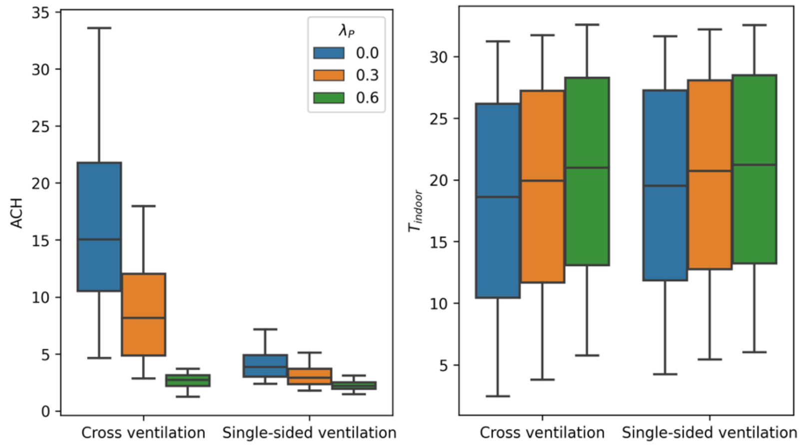

Fig. 14. Annual variability in upper floor air changes per hour (ACH) (left) and indoor air temperature (right) but for Shanghai for two ventilation modes.

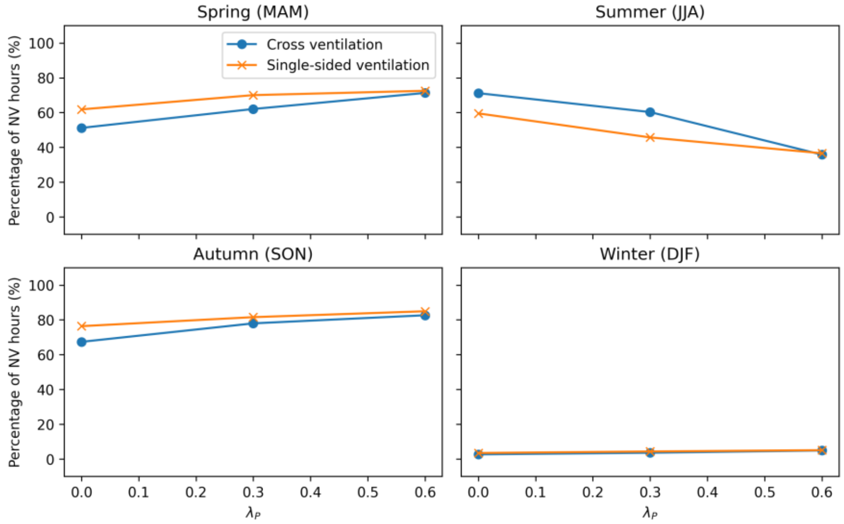

Fig. 15. Seasonal upper floor with cross ventilation (**percentage of NV hours**) in Shanghai for two ventilation modes.

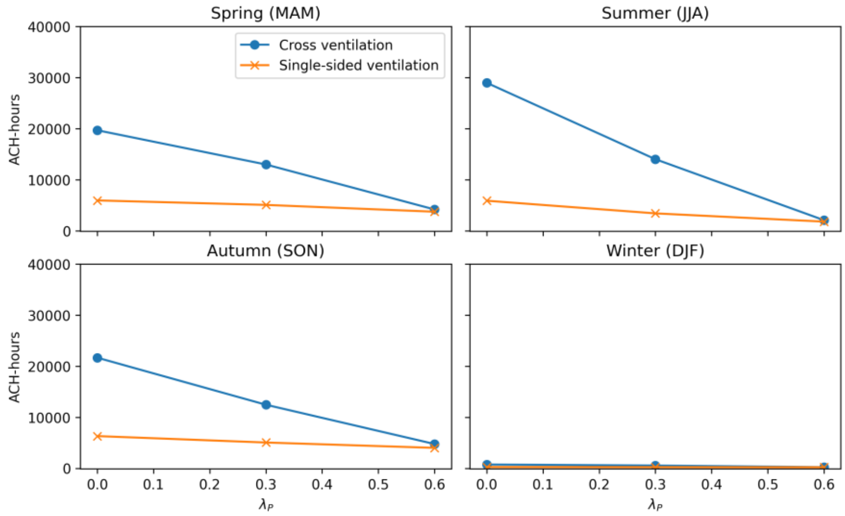

Fig. 16. Seasonal upper floor **ACH-hours** with cross ventilation in Shanghai for two ventilation modes.

3.3. Cooling energy saving

The cooling energy saving is calculated as the difference in cooling energy demand between a building with air-conditioning only and hybrid ventilation (air-conditioning plus natural ventilation). Therefore, the cooling energy saving amount is linked with the effectiveness of natural ventilation cooling (Eq. 10). Cooling energy saving is expected to be larger for climates and neighbourhoods with lower outdoor air temperatures and higher wind speeds. Hence, in all climates the cooling energy saving decreases as λ_P increases (Fig. 17). For cross ventilation, such decreases are smallest in Kunming, as the climate is mild and temperature variation is small, making natural ventilation cooling available most of the time. For the other climates the cooling energy saving between building densities (λ_P) are similar (Harbin: 8% to Beijing: 12.5%).

Our results differ slightly from Ramponi et al. (2014)'s nocturnal ventilation cooling energy saving study of three European cities. They suggest inter-λ_P differences are largely influenced by the climate, with natural ventilation cooling energy saving dropping by 20% in cool but windy Amsterdam, while in warmer less windy Milan (2 %) and Rome (13 %) reductions are less. Differences may arise from their different approach, as their outdoor air temperatures and wind speeds are independent of λ_P (only C_p values changed), and longwave radiative exchanges are not considered. The last may be critical as increased λ_P can result in more trapped longwave radiation, increasing building cooling demand (Xie et al. 2022). Our work highlights the importance of a holistic consideration of the complex interaction between urban climate and building performance.

Compared to cross ventilation, single-sided ventilation has less cooling energy savings due to lower wind speeds. The trends across climates are similar, despite slightly smaller inter- λ_P variations (6.5% to 8.1% excluding Kunming).

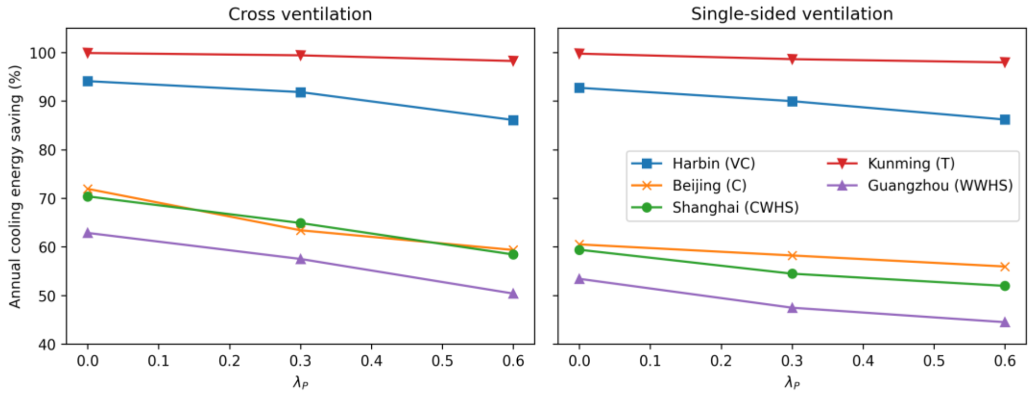

Fig. 17. Seasonal upper floor with cross ventilation annual **cooling energy saving** (Eq. 10, percentages) in five climates (colour) and two ventilation modes.

4. Discussion and conclusions

Although NVP across China's climate zones has been assessed previously, given the large dependence on research approach, climate data and building model used, the results vary (Luo et al., 2007; Tong et al., 2016; Yang et al., 2005; Yao et al., 2009). However, the urban factors influencing buildings in an urban environment are often not fully considered.

In this study, we propose a multi-scale modelling scheme that combines the urban land surface model SUEWS and building energy simulation tool EnergyPlus to assess the natural ventilation potential (NVP) of buildings in different Chinese climate zones and neighbourhoods with different building plan area fractions (λ_P). Unlike traditional approaches that treat buildings as being isolated and use rural weather data, our approach considers multiple urban factors, including the influence of the urban neighbourhood morphology on canopy air temperature, wind sheltering effects, overshadowing, and longwave radiative exchanges. Compared to computationally intensive methods like CFD, our approach offers practical advantages in terms of simplicity and computational cost. The SUEWS model only requires some commonly available surface characteristics and meteorological forcing data. A year long run for one neighbourhood normally takes around 1 minute (PC) which is around 10^6 times less than CFD-based approaches (e.g. 3-day run taking 168 hours on PC by Yang et al. (2012)). Therefore, our approach can be applied for quick estimates of natural ventilation potential and cooling energy saving in larger scales (e.g. intra-city neighbourhoods) for longer time periods. Also, the outputs by SUEWS can be used as boundary conditions for CFD simulation.

We find that climate, plan area fraction and season combine to impact the NVP. Our findings improve current understanding and design of NVP of urban buildings from a local climate perspective. Local climate in denser areas have been shown to reduce NVP due to warmer outdoor air temperatures on several summer days in Basel (cf. the rural area) (Germano, 2007) and reduced wind speeds from increasing λ_P ($0 \rightarrow 0.2$) reducing annual mean wind-driven ventilation rate by up to 35% (Li and Li, 2015). Given these studies, our findings further suggest that under different conditions, increasing the λ_P can either increase or decrease the NVP. For example, in summer, when the λ_P increases from 0 to 0.6, NV-hours increase by around 10% in Harbin (very cold) but decrease by around 43% in Guangzhou (warm winter hot summer). However, a critical disadvantage of urban areas is the low wind speeds, which leads to lower ventilation rates (e.g. Harbin: annual median ventilation rate reduced by 50% at λ_P =0.3 and 85% at λ_P =0.6). Hence, we should consider both NV-hours and ACH-hours. It is also found that single-sided ventilation can be as effective as cross ventilation in dense urban areas due to the low wind speed regardless of the metric used.

In this study we consider three metrics: NV-hour, ACH-hour, and cooling energy saving. The NV-hour, commonly used to measure NVP, gives the duration (in hours) suitable for natural ventilation. This metric is appropriate when considering general buildings without specific ventilation requirements. Limitation of the NV-hour metric includes its primarily reliance on thermal comfort based on indoor temperature and considers only a minimum ventilation rate limit, disregarding variations in ventilation rates determined by wind speed. To address this limitation, we introduce the ACH-hour, which incorporates ventilation rates based on the NV-hour and accounts for the influence of wind speed. The ACH-hour can offset the impact of temperature by considering high wind speeds and larger ventilation rates. For instance, even though Kunming has a milder climate and more NV-hours, the annual ACH-hours in Harbin are greater at λ_P = 0. Additionally, ACH-hours consistently decrease as λ_P increases. Therefore, the ACH-hour is more appropriate when ventilation rate is a critical factor. Whilst, the cooling energy saving metric (units: %) is influenced by both NVP and the original cooling demand. Climates with cooler summers, such as Harbin and Kunming, have higher percentages of cooling energy saving. This metric is particularly relevant for buildings with mixed-mode ventilation systems. Hence, these metrics are useful for different applications when considering the building and climate being evaluated.

Our approach offers a quick assessment of NVP for buildings in the urban environment. We model idealised neighbourhoods with simplified building models based on relevant observations and standards, although we acknowledge that real cities are more complex. Natural ventilation depends on factors like building and room geometry. In this study we use a simplified shoebox model without interior partitions to maximise cross-ventilation, but real buildings with multiple rooms may have lower cross-ventilation rates, approaching single-sided ventilation. Hence, in more realistic scenarios, NVP for cross-ventilation may resemble that of single-sided ventilation.

Additionally, we assume consistent human activities across regions, overlooking any resulting modifications to anthropogenic heat emissions. Local socioeconomic conditions and population density cause large intra-city emission variability. In our study the neighbourhood density accounted for but not the overall inter-city differences in mean city-wide population density. The latter vary from > 2000 per km^2 in Shanghai to around 900 per km^2 in Kunming (Xu et al., 2019). Higher population densities often correspond to increased anthropogenic heat emissions, resulting in higher urban air temperatures that affect NVP. Densely populated neighbourhoods can have greater anthropogenic heat emissions due to increased building energy consumption and traffic-related emissions. Accounting for these variables can impact NVP results. Detailed data can be used to model anthropogenic heat emissions in different neighbourhoods using SUEWS.

Our findings should be representative of similar climates and neighbourhoods, but future studies could focus on more detailed information on neighbourhoods in real cities where the variance in NVP might be greater. Existing evaluations suggest that the SUEWS model has acceptable accuracy, although the C_p values should be changed with building geometry. We have only considered buildings and grass in our study and have ignored the impact of trees, which could modify the wind field (Kent et al., 2018) and radiative fluxes (Morrison et al., 2018) and affect the natural ventilation of nearby buildings. Although trees can be modelled in SUEWS and considered as shading objects in EnergyPlus (e.g. Hsieh et al., 2018), to modify wind pressure coefficients on nearby building facets, measurements or CFD simulations are still necessary. Therefore, our approach can be extended with additional data. Additionally, air and noise pollution, which could be high in dense urban areas, may further reduce NVP (as noted in Table 1), but this is beyond the scope of this study and could be considered in future work.

5. **Acknowledgement** This work has been funded as part of NERC-COSMA (NE/S005889/1) and ERC urbisphere (855005).

6. **Data availability** Information on the data underpinning the results presented here can be found at https://doi.org/10.5281/zenodo.7802864 (Xie et al., 2023).

7. References

Allen, L., Lindberg, F., Grimmond, C.S.B., 2011. Global to city scale urban anthropogenic heat flux: model and variability. Int. J. Climatol. 31, 1990–2005.

Anđelković, A.S., Mujan, I., Dakić, S., 2016. Experimental validation of a EnergyPlus model: Application of a multi-storey naturally ventilated double skin façade. Energy Build. 118, 27–36.

ANSI/ASHRAE, 2011. Standard Method of Test for the Evaluation of Building Energy Analysis Computer Programs. Atlanta.

ANSI/ASHRAE, 2013. Ventilation for Acceptable Indoor Air Quality.

ASHRAE, 2005. ASHRAE Handbook : Fundamentals. American Society of Heating, Refrigerating and Air-Conditioning Engineers, Atlanta.

Augusto, B., Roebeling, P., Rafael, S., Ferreira, J., Ascenso, A., Bodilis, C., 2020. Short and medium- to long-term impacts of nature-based solutions on urban heat. Sustain. Cities Soc. 57, 102122.

Awbi, H.B., 2003. Ventilation of Buildings, Second. ed. Taylor & Francis Group, New York.

Aynsley, R., 1999. Estimating summer wind driven natural ventilation potential for indoor thermal comfort. J. Wind Eng. Ind. Aerodyn. 83, 515–525.

Boccalatte, A., Fossa, M., Gaillard, L., Menezo, C., 2020. Microclimate and urban morphology effects on building energy demand in different European cities. Energy Build. 224, 110129.

CABEE, 2021. China Building Energy Consumption and Carbon Emission Research Report.

Causone, F., 2016. Climatic potential for natural ventilation. Archit. Sci. Rev. 59, 212–228.

Chen, Y., Tong, Z., Malkawi, A., 2017. Investigating natural ventilation potentials across the globe: Regional and climatic variations. Build. Environ. 122, 386–396.

Chen, Y., Tong, Z., Wu, W., Samuelson, H., Malkawi, A., Norford, L., 2019. Achieving natural ventilation potential in practice: Control schemes and levels of automation. Appl. Energy 235, 1141–1152.

Cheng, J., Qi, D., Katal, A., Wang, L., Stathopoulos, T., 2018. Evaluating wind-driven natural ventilation potential for early building design.

Cheng, Z., Li, L., Bahnfleth, W.P., 2016. Natural ventilation potential for gymnasia – Case study of ventilation and comfort in a multisport facility in northeastern United States. Build. Environ. 108, 85–98.

Costanzo, V., Yao, R., Xu, T., Xiong, J., Zhang, Q., Li, B., 2019. Natural ventilation potential for residential buildings in a densely built-up and highly polluted environment. A case study. Renew. Energy 138, 340–353.

Emmerich, S.J., Dols, W.S., Axley, J.W., 2001. Natural ventilation review and plan for design and analysis tools. National Institute of Standards and Technology, Gaithersburg.

Faggianelli, G.A., Brun, A., Wurtz, E., Muselli, M., 2014. Natural cross ventilation in buildings on Mediterranean coastal zones. Energy Build. 77, 206–218.

Fernández, M.E., Picone, N., Gentili, J.O., Campo, A.M., 2021. Analysis of the Urban Energy Balance in Bahía Blanca (Argentina). Urban Clim. 37, 100856.

Fumo, N., Mago, P., Luck, R., 2010. Methodology to estimate building energy consumption using EnergyPlus Benchmark Models. Energy Build. 42, 2331–2337.

Germano, M., 2007. Assessing the natural ventilation potential of the Basel region. Energy Build. 39, 1159–1166.

Ghiaus, C., Allard, F., Santamouris, M., Georgakis, C., Nicol, F., 2006. Urban environment influence on natural ventilation potential. Build. Environ. 41, 395–406.

Gough, H.L., Barlow, J.F., Luo, Z., King, M.F., Halios, C.H., Grimmond, C.S.B., 2020. Evaluating single-sided natural ventilation models against full-scale idealised measurements: Impact of wind direction and turbulence. Build. Environ. 170, 106556.

Grimmond, C.S.B., Blackett, M., Best, M.J., Baik, J.-J., Belcher, S.E., Beringer, J., Bohnenstengel, S.I., Calmet, I., Chen, F., Coutts, A., Dandou, A., Fortuniak, K., Gouvea, M.L., Hamdi, R., Hendry, M., Kanda, M., Kawai, T., Kawamoto, Y., Kondo, H., Krayenhoff, E.S., Lee, S.-H., Loridan, T., Martilli, A., Masson, V., Miao, S., Oleson, K., Ooka, R., Pigeon, G., Porson, A., Ryu, Y.-H., Salamanca, F., Steeneveld, G.J., Tombrou, M., Voogt, J.A., Young, D.T., Zhang, N., 2011. Initial results from Phase 2 of the international urban energy balance model comparison. Int. J. Climatol. 31, 244–272.

Grimmond, C.S.B., Blackett, M., Best, M.J., Barlow, J., Baik, J.J., Belcher, S.E., Bohnenstengel, S.I., Calmet, I., Chen, F., Dandou, A., Fortuniak, K., Gouvea, M.L., Hamdi, R., Hendry, M., Kawai, T., Kawamoto, Y., Kondo, H., Krayenhoff, E.S., Lee, S.H., Loridan, T., Martilli, A., Masson, V., Miao, S., Oleson, K., Pigeon, G., Porson, A., Ryu, Y.H., Salamanca, F., Shashua-Bar, L., Steeneveld, G.J., Tombrou, M., Voogt, J., Young, D., Zhang, N., 2010. The International Urban Energy Balance Models Comparison Project: First Results from Phase 1. J. Appl. Meteorol. Climatol. 49, 1268–1292.

Grimmond, C.S.B., Oke, T.R., 1999a. Heat Storage in Urban Areas: Local-Scale Observations and Evaluation of a Simple Model. J. Appl. Meteorol. 38, 922–940.

Grimmond, C.S.B., Oke, T.R., 1999b. Aerodynamic Properties of Urban Areas Derived from Analysis of Surface Form. J. Appl. Meteorol. 38, 1262–1292.

Grimmond, C.S.B., Oke, T.R., Steyn, D.G., 1986. Urban Water Balance: 1. A Model for Daily Totals. Water Resour. Res. 22, 1397–1403.

Grosso, M., 1992. Wind pressure distribution around buildings: a parametrical model. Energy Build. 18, 101–131.

Harman, I.N., Finnigan, J.J., 2007. A simple unified theory for flow in the canopy and roughness sublayer. Boundary-Layer Meteorol. 123, 339–363.

Harman, I.N., Finnigan, J.J., 2008. Scalar Concentration Profiles in the Canopy and Roughness Sublayer. Boundary-Layer Meteorol. 129, 323–351.

Havu, M., Kulmala, L., Kolari, P., Vesala, T., Riikonen, A., Järvi, L., 2022. Carbon sequestration potential of street tree plantings in Helsinki. Biogeosciences 19, 2121–2143.

Hensen, J.L.M. (Jan), 1999. Simulation of building energy and indoor environmental quality - Some weather data Issues. Int. Work. Clim. data their Appl. Eng. 1–15.

Hersbach, H., Bell, B., Berrisford, P., Hirahara, S., Horányi, A., Muñoz-Sabater, J., Nicolas, J., Peubey, C., Radu, R., Schepers, D., Simmons, A., Soci, C., Abdalla, S., Abellan, X., Balsamo, G., Bechtold, P., Biavati, G., Bidlot, J., Bonavita, M., De Chiara, G., Dahlgren, P., Dee, D., Diamantakis, M., Dragani, R., Flemming, J., Forbes, R., Fuentes, M., Geer, A., Haimberger, L., Healy, S., Hogan, R.J., Hólm, E., Janisková, M., Keeley, S., Laloyaux, P., Lopez, P., Lupu, C., Radnoti, G., de Rosnay, P., Rozum, I., Vamborg, F., Villaume, S., Thépaut, J.N., Muñoz-Sabater, J., Nicolas, J., Peubey, C., Radu, R., Schepers, D., Simmons, A., Soci, C., Abdalla, S., Abellan, X., Balsamo, G., Bechtold, P., Biavati, G., Bidlot, J., Bonavita, M., Chiara, G., Dahlgren, P., Dee, D., Diamantakis, M., Dragani, R., Flemming, J., Forbes, R., Fuentes, M., Geer, A., Haimberger, L., Healy, S., Hogan, R.J., Hólm, E., Janisková, M., Keeley, S., Laloyaux, P., Lopez, P., Lupu, C., Radnoti, G., Rosnay, P., Rozum, I., Vamborg, F., Villaume, S., Thépaut, J.N., 2020. The ERA5 global reanalysis. Q. J. R. Meteorol. Soc. 146, 1999–2049.

Hiyama, K., Glicksman, L., 2015. Preliminary design method for naturally ventilated buildings using target air change rate and natural ventilation potential maps in the United States.

Hsieh, C.-M., Li, J.-J., Zhang, L., Schwegler, B., 2018. Effects of tree shading and transpiration on building cooling energy use. Energy Build. 159, 382–397.

Integrated Environmental Solutions, 2018. MacroFlo calculation methods [WWW Document]. URL https://help.iesve.com/ve2018/ (accessed 6.30.22).

Järvi, L., Grimmond, C.S.B., Christen, A., 2011. The Surface Urban Energy and Water Balance Scheme (SUEWS): Evaluation in Los Angeles and Vancouver. J. Hydrol. 411, 219–237.

Johnson, M.H., Zhai, Z.J., Krarti, M., 2012. Performance evaluation of network airflow models for natural ventilation, HVAC and R Research.

Kamal, A., Abidi, S.M.H., Mahfouz, A., Kadam, S., Rahman, A., Hassan, I.G., Wang, L.L., 2021. Impact of urban morphology on urban microclimate and building energy loads. Energy Build. 253, 111499.

Kent, C.W., Lee, K., Ward, H.C., Hong, J.-W., Hong, J., Gatey, D., Grimmond, S., 2018. Aerodynamic roughness variation with vegetation: analysis in a suburban neighbourhood and a city park. Urban Ecosyst. 21, 227–243.

Lam, K.P., Zhao, J., Ydstie, E.B., Wirick, J., Qi, M., Park, J., 2014. An EnergyPlus whole building energy model calibration method for office buildings using occupant behavior data mining and empirical data. In: 2014 ASHRAE/IBPSA-USA Building Simulation Conference. pp. 160–167.

Li, Y., Li, X., 2015. Natural ventilation potential of high-rise residential buildings in northern China using coupling thermal and airflow simulations. Build. Simul. 8, 51–64.

Lindberg, F., Grimmond, C.S.B., Gabey, A., Huang, B., Kent, C.W., Sun, T., Theeuwes, N.E., Järvi, L., Ward, H.C., Capel-Timms, I., Chang, Y., Jonsson, P., Krave, N., Liu, D., Meyer, D., Olofson, K.F.G., Tan, J., Wästberg, D., Xue, L., Zhang, Z., 2018. Urban Multi-scale Environmental Predictor (UMEP): An integrated tool for city-based climate services. Environ. Model. Softw. 99, 70–87.

Lindberg, F., Olofson, K.F.G., Sun, T., Grimmond, C.S.B., Feigenwinter, C., 2020. Urban storage heat flux variability explored using satellite, meteorological and geodata. Theor. Appl. Climatol. 141, 271–284.

Liu, J., Li, Y., Zhang, C., Liu, Z., 2022. The effect of high altitude environment on diesel engine performance: Comparison of engine operations in Hangzhou, Kunming and Lhasa cities. Chemosphere 309, 136621.

Liu, Y., Stouffs, R., Tablada, A., Wong, N.H., Zhang, J., 2017. Comparing micro-scale weather data to building energy consumption in Singapore. Energy Build. 152, 776–791.

Luo, Z., Zhao, J., Gao, J., He, L., 2007. Estimating natural-ventilation potential considering both thermal comfort and IAQ issues. Build. Environ. 42, 2289–2298.

Magli, S., Lodi, C., Lombroso, L., Muscio, A., Teggi, S., 2015. Analysis of the urban heat island effects on building energy consumption. Int. J. Energy Environ. Eng. 6, 91–99.

Martins, N.R., Carrilho Da Graça, G., 2017. Simulation of the effect of fine particle pollution on the potential for natural ventilation of non-domestic buildings in European cities.

Mei, S.J., Hu, J.T., Liu, D., Zhao, F.Y., Li, Y., Wang, Y., Wang, H.Q., 2017. Wind driven natural ventilation in the idealized building block arrays with multiple urban morphologies and unique package building density. Energy Build. 155, 324–338.

MoHURD, 2012. Evaluation standard for indoor thermal environment in civil buildings (GB/T50785-2012). Ministry of Housing and Urban-rural Development, P.R. China, Beijing.

MoHURD, 2015. Design standard for energy efficiency of public buildings (GB50189-2015). Ministry of Housing and Urban-rural Development, P.R. China, Beijing.

MoHURD, 2016. Code for thermal design of civil building (GB50176-2016). Ministry of Housing and Urban-rural Development, P.R. China, Beijing.

Morrison, W., Kotthaus, S., Grimmond, C.S.B., Inagaki, A., Yin, T., Gastellu-Etchegorry, J.P., Kanda, M., Merchant, C.J., 2018. A novel method to obtain three-dimensional urban surface temperature from ground-based thermography. Remote Sens. Environ. 215, 268–283.

Nicol, F., Humphreys, M., 2010. Derivation of the adaptive equations for thermal comfort in free-running buildings in European standard EN15251. Build. Environ. 45, 11–17.

Oke, T.R., Mills, G., Christen, A., Voogt, J.A., 2017a. Urban Climates. Cambridge University Press, Cambridge.

Oke, T.R., Mills, G., Christen, A., Voogt, J.A., 2017b. Urban climates. Cambridge University Press, Cambridge.

Oropeza-Perez, I., Østergaard, P.A., 2013. Potential of natural ventilation in temperate countries-A case study of Denmark.

Patil, K.N., Kaushik, S.C., 2015. Study of climatic potential for natural ventilation in buildings for typical Indian cities. Int. J. Vent. 13, 369–380.

Pesic, N., Roset Calzada, J., Muros Alcojor, A., 2018. Natural ventilation potential of the Mediterranean coastal region of Catalonia. Energy Build. 169, 236–244.

Rafael, S., Martins, H., Matos, M.J., Cerqueira, M., Pio, C., Lopes, M., Borrego, C., 2020. Application of SUEWS model forced with WRF: Energy fluxes validation in urban and suburban Portuguese areas. Urban Clim. 33, 100662.

Ramponi, R., Gaetani, I., Angelotti, A., 2014. Influence of the urban environment on the effectiveness of natural night-ventilation of an office building. Energy Build. 78, 25–34.

Royapoor, M., Roskilly, T., 2015. Building model calibration using energy and environmental data. Energy Build. 94, 109–120.

Ryan, E.M., Sanquist, T.F., 2012. Validation of building energy modeling tools under idealized and realistic conditions. Energy Build. 47, 375–382.

Sailor, D.J., 2011. A review of methods for estimating anthropogenic heat and moisture emissions in the urban environment. Int. J. Climatol. 31, 189–199.

Sakiyama, N.R.M., Mazzaferro, L., Carlo, J.C., Bejat, T., Garrecht, H., 2021. Natural ventilation potential from weather analyses and building simulation. Energy Build. 231, 110596.

Sun, T., Grimmond, S., 2019. A Python-enhanced urban land surface model SuPy (SUEWS in Python, v2019.2): Development, deployment and demonstration. Geosci. Model Dev. 12, 2781–2795.

Sun, T., Järvi, L., Omidvar, H., Theeuwes, N., Lindberg, F., Li, Z., Grimmond, S., 2020. Urban-Meteorology-Reading/SUEWS: 2020a Release.

Sundell, J., Levin, H., Nazaroff, W.W., Cain, W.S., Fisk, W.J., Grimsrud, D.T., Gyntelberg, F., Li, Y., Persily, A.K., Pickering, A.C., Samet, J.M., Spengler, J.D., Taylor, S.T., Weschler, C.J., 2011. Ventilation rates and health: multidisciplinary review of the scientific literature. Indoor Air 21, 191–204.

Tan, Z., Deng, X., 2017. Assessment of natural ventilation potential for residential buildings across different climate zones in Australia. Atmosphere (Basel). 8, 177.

Tang, Y., Sun, T., Luo, Z., Omidvar, H., Theeuwes, N., Xie, X., Xiong, J., Yao, R., Grimmond, S., 2021. Urban meteorological forcing data for building energy simulations. Build. Environ. 204, 108088.

Theeuwes, N.E., Ronda, R.J., Harman, I.N., Christen, A., Grimmond, C.S.B., 2019. Parametrizing horizontally-averaged wind and temperature profiles in the urban roughness sublayer. Boundary-Layer Meteorol. 173, 321–348.

Tong, Z., Chen, Y., Malkawi, A., 2017. Estimating natural ventilation potential for high-rise buildings considering boundary layer meteorology. Appl. Energy 193, 276–286.

Tong, Z., Chen, Y., Malkawi, A., Liu, Z., Freeman, R.B., 2016. Energy saving potential of natural ventilation in China: The impact of ambient air pollution. Appl. Energy 179, 660–668.

Toparlar, Y., Blocken, B., Maiheu, B., van Heijst, G.J.F., 2017. A review on the CFD analysis of urban microclimate. Renew. Sustain. Energy Rev. 80, 1613–1640.

TPU, 2007. Aerodynamic database for low-rise buildings. Tokyo, Japan.

TRNSYS, 2009. TRNSYS 17: Mathematical reference.

U.S. Department of Energy, 2020a. Chapter 1: Overview. In: EnergyPlus Version 9.4.0 Documentation: Engineering Reference. pp. 20–24.

U.S. Department of Energy, 2020b. Chapter 13: Alternative modeling processes. In: EnergyPlus Version 9.4.0 Documentation: Engineering Reference. pp. 601–705.

U.S. Department of Energy, 2020c. Chapter 8: Air Heat Balance Manager / Processes. In: EnergyPlus Version 9.4.0 Documentation: Engineering Reference. pp. 58–168.

U.S. Department of Energy, 2020d. Chapter 5: Climate, Sky and Solar/Shading Calculations. In: EnergyPlus Version 9.4.0 Documentation: Engineering Reference. pp. 187–224.

UN, 2015. Paris Agreement.

UNEP, 2020. 2020 Global Status Report for Buildings and Construction: Towards a Zero-emission, Efficient and Resilient Buildings and Construction Sector. Nairobi.

van Hooff, T., Blocken, B., 2010. On the effect of wind direction and urban surroundings on natural ventilation of a large semi-enclosed stadium. Comput. Fluids 39, 1146–1155.

van Hooff, T., Blocken, B., Tominaga, Y., 2017. On the accuracy of CFD simulations of cross-ventilation flows for a generic isolated building: Comparison of RANS, LES and experiments. Build. Environ. 114, 148–165.

Wang, B., Malkawi, A., 2019. Design-based natural ventilation evaluation in early stage for high performance buildings. Sustain. Cities Soc. 45, 25–37.

Ward, H.C., Grimmond, C.S.B., 2017. Assessing the impact of changes in surface cover, human behaviour and climate on energy partitioning across Greater London. Landsc. Urban Plan. 165, 142–161.

Ward, H.C., Kotthaus, S., Järvi, L., Grimmond, C.S.B., 2016. Surface Urban Energy and Water Balance Scheme (SUEWS): Development and evaluation at two UK sites. Urban Clim. 18, 1–32.

Warren, P.R., 1977. Ventilation through openings on one wall only. In: International Conference on Heat and Mass Transfer in Buildings. Dubrovnik.

Warren, P.R., Parkins, L.M., 1984. Single-sided ventilation through open windows. In: Document - Swedish Council for Building Research. p. 487.

Wiegels, R., Chapa, F., Hack, J., 2021. High resolution modeling of the impact of urbanization and green infrastructure on the water and energy balance. Urban Clim. 39, 100961.

WMO, 2023. Guidance to Measuring, Modelling and Monitoring the Canopy Layer Urban Heat Island, EMS Annual Meeting 2021. Geneva.

Xie, X., Luo, Z., Grimmond, S., Blunn, L., 2023. Use of wind pressure coefficients to simulate natural ventilation and building energy for isolated and surrounded buildings. Build. Environ. 230, 109951.

Xie, X., Luo, Z., Grimmond, S., Sun, T., Morrison, W., 2022. Impact of inter-building longwave radiative exchanges on building energy performance and indoor overheating. Build. Environ. 209, 108628.

Xiong, J., Yao, R., Grimmond, S., Zhang, Q., Li, B., 2019. A hierarchical climatic zoning method for energy efficient building design applied in the region with diverse climate characteristics. Energy Build. 186, 355–367.

Xu, G., Jiao, L., Yuan, M., Dong, T., Zhang, B., Du, C., 2019. How does urban population density decline over time? An exponential model for Chinese cities with international comparisons. Landsc. Urban Plan. 183, 59–67.

Xu, K., Lu, R., Mao, J., Chen, R., Ke, X.U., Riyu, L.U., Jiangyu, M., Ruidan, C., 2019. Circulation anomalies in the mid–high latitudes responsible for the extremely hot summer of 2018 over northeast Asia. New pub KeAi 12, 231–237.

Yamanaka, T., Kotani, H., Iwamoto, K., Kato, M., 2006. Natural, wind-forced ventilation caused by turbulence in a room with a single opening. Int. J. Vent.

Yan, D., Xia, J., Tang, W., Song, F., Zhang, X., Jiang, Y., 2008. DeST — An integrated building simulation toolkit Part I: Fundamentals. Build. Simul. 2008 12 1, 95–110.

Yang, L., Zhang, G., Li, Y., Chen, Y., 2005. Investigating potential of natural driving forces for ventilation in four major cities in China. Build. Environ. 40, 738–746.

Yang, W., Quan, Y., Jin, X., Tamura, Y., Gu, M., 2008. Influences of equilibrium atmosphere boundary layer and turbulence parameter on wind loads of low-rise buildings. J. Wind Eng. Ind. Aerodyn. 96, 2080–2092.

Yang, X., Zhao, L., Bruse, M., Meng, Q., 2012. An integrated simulation method for building energy performance assessment in urban environments. Energy Build. 54, 243–251.

Yao, R., Li, B., Steemers, K., Short, A., 2009. Assessing the natural ventilation cooling potential of office buildings in different climate zones in China. Renew. Energy 34, 2697–2705.

Yin, W., Zhang, G., Yang, W., Wang, X., 2010. Natural ventilation potential model considering solution multiplicity, window opening percentage, air velocity and humidity in China. Build. Environ. 45, 338–344.

Yoon, N., Norford, L., Malkawi, A., Samuelson, H., Piette, M.A., 2020. Dynamic metrics of natural ventilation cooling effectiveness for interactive modeling. Build. Environ. 180, 106994.

Zhai, Z. (John), Johnson, M.H., Mankibi, M. El, Stathopoulos, N., 2016. Review of natural ventilation models. Int. J. Vent. 15, 186–204.

Zhang, A., Gao, C., Zhang, L., 2005. Numerical simulation of the wind field around different building arrangements. J. Wind Eng. Ind. Aerodyn. 93, 891–904.

Zhong, H.Y., Sun, Y., Shang, J., Qian, F.P., Zhao, F.Y., Kikumoto, H., Jimenez-Bescos, C., Liu, X., 2022. Single-sided natural ventilation in buildings: a critical literature review. Build. Environ. 212.